RSC Advances

ROYAL SOCIETY OF CHEMISTRY

www.rsc.org/advances

Cite this: DOI: 10.1039/c0xx00000x

www.rsc.org/xxxxxx

ARTICLE TYPE

Orthogonal Experimentation for Optimization of TiO_2 Nanoparticles Hydrothermal Synthesis and Photocatalytic Property of TiO_2/Concrete Composite

JianlinLuo*[a], Guixian Zhu[a], Fangfang Zhang[a,b], Qiuyi Li[a], Tiejun Zhao[a], and Xueqing Zhu[a]

Received (in XXX, XXX) Xth XXXXXXXXX 20XX, Accepted Xth XXXXXXXXX 20XX
DOI: 10.1039/b000000x

Orthogonal experimental design was applied to optimize the hydrothermal preparation parameters of TiO_2 nanoparticles by the analysis of means (*ANOM*) and variances (*ANOVA*). The ANOM & ANOVA results on crystalline and size show that the optimal process of synthesized TiO_2 nanoparticles is 5.0% TBT, alkalescent environment (pH=9), 160 °C reaction temperature, and 3 hrs reaction time. The main factors affecting on the photocatalytic properties of TiO_2 nanoparticles were explored by measuring UV light absorbance index, the results show that their photocatalytic performance are excellent when methyl orange (MeO) concentration is 2.5mg/L, pH value is 6, the Ag-doped amount is 5.0%. Then optimal TiO_2 nanoparticles aqueous suspensions with varied concentration (c_{TiO2}) were sprayed on the permeable concretes to fabricate TiO_2/concrete composites, and their photocatalytic activity was evaluated by measuring degradation rate of soaked MeO along the UV radiation time. It is concluded that when c_{TiO2} is 2.0 g/L with fixed above conditions, the produced TiO_2/concrete composite has an optimal capacity (35.7%) in photo-degradation of azo pollutants.

1. Introduction

Air pollution caused by exhaust emissions and industry has increasingly drawn public attention, especially in urban areas. Traditional emission reduction systems might not realize complete degradation of nitric oxides from motor vehicles and industrial waste.

Titanium dioxide (TiO_2) is a semiconductor material characterized by its valence and conduction band energy positions.[1] TiO_2 is the most applied photocatalyst since the end of the 1980s, which is attributed to its two main qualities: self-cleaning effect and photo-induced surface hydrophilicity.[2] After initiated by sunlight activation (usually UV light), the photo-excited electron-hole pairs will promote oxidation and reduction of exhaust gases (just like (NO_x)[3]) and toxic organic pollutants[4] and transform them into nontoxic molecules (in general, H_2O and CO_2). The generated hydrophilic surface might efficiently prevent stains and dirt from staying on the TiO_2 surface.

There were various methods about TiO_2 nanoparticles preparation.[5] Compared with other synthetic methods, the hydrothermal method has prominent advantages, one of them is that highly mono-dispersed TiO_2 nanoparticles are directly synthesized.[6] This avoids of sintering process, which may not accurately control TiO_2 crystalline structure. By adjusting hydrothermal conditions (such as temperature, pH value, stress and reaction time), a variety of TiO_2 nanoparticles can be formed with different morphology, crystal structure and particle size.

Municipal infrastructure guardrail and external building concrete surfaces are the optimal media for applying photocatalytic materials to reduce air pollution in urban areas.[7] The high surface areas of lightweight porous concrete offers ample interface to TiO_2 and pollutant molecules. As a main protective part of urban construction, porous concretes may have a potential to be self-clean and air purifying properties.[8] TiO_2 addition is also capable of improving strength, resistance to water permeability and reducing fracture areas of porous concretes.[9] Therefore, if combined with TiO_2 with superior photocatalytic activity, the fabricated TiO_2/concrete composite might have improved self-performances and environment quality through light degradation of pollutants (toxic organics and exhaust gas) by TiO_2 nanoparticles.

Anatase-type TiO_2 has been proved possessing more excellent photocatalytic property compared with rutile and brookite-type. Apart from its crystalline phase, size is another main element to influence TiO_2's catalytic activity. Orthogonal experiment is effective to evaluate the relative importance of different factors on a response and find out the optimal levels for different factors by applying orthogonal arrays, while dramatically reducing testing time and cost.

In this paper, in order to find out optimal size and crystalline about TiO_2, orthogonal experiment method assembled with four factors (temperature, pH value, Tetra-*n* butyl titanate (TBT) concentration and reaction time), one at three levels was applied to design factors composition through $OA_9(3^4)$ table, which may realize efficient elements ratio. Crystalline phase and size of prepared TiO_2 nanoparticles were characterized by a XRD and laser scattering particle analyzer, respectively. Then

consequences were analyzed by analysis of mean (*ANOM*) and variance (*ANOVA*) in order to identify optimal parameter ratio.

Subsequently, the optimal synthesized TiO_2 nanoparticles were dispersed in aqueous suspension by surfactant ultrasonic method, and then directly sprayed on permeable concrete surface to produce TiO_2/concrete composite. Then photocatalytic properties of the formed TiO_2 nanoparticles and TiO_2/concrete composite were characterized through their oxidation of soaked methyl orange solutions under UV radiation.

2. Experimental details

2.1 Raw materials

Tetra-*n*-butyl titanate ($C_4H_9O)_4Ti$) (TBT, AR), was purchased from China Sun Specialty Products Co., Ltd.; Absolute ethyl alcohol (C_2H_5OH), using as the main solvent, was bought from Far Eastern Group, China; Ammonia (AR) and acetic acid (AR), using for pH regulation, were acquired from Laiyang Kangde and Tianjing Hengxing Chemical Co., Ltd., China, respectively; Methyl orange (MeO), which is applied in photo-degradation assay, was obtained from Tianjing Hengxing Chemical Co., Ltd., China; Silver nitrate (AR), using as the dopant, was purchased from Shanghai Aibi Chemistry Preparation Co., Ltd, China; Both Triton x100 (AR, imported subpackage) using as dispersing aid and sodium aluminate (AR) using as cement setting accelerator were purchased from Sinopharm Chemical Reagent Co., Ltd., China; Hydrogen peroxide solution (H_2O_2, 30%), using as the foaming agent, was purchased from Tianjin Guangcheng Chemical Reagent Co. Ltd., China; The ordinary Portland cement (P.O. 42.5R, conforming to ASTM Type I) was purchased from SUNNSY Shanshui Cement Group Ltd., China, its chemical composition is listed in Table 1; Distilled water, commercial available.

Table 1 Main chemical composition of ordinary Portland cement (wt.%).

CaO	SiO_2	Al_2O_3	Fe_2O_3	MgO	SO_3	IL
61.70	20.10	5.09	2.93	1.58	1.99	1.75

2.2 Synthesis of TiO_2 nanoparticles & orthogonal test design

TBT solution was firstly dissolved in ethyl alcohol (the amount of total solution was 100 g); The ammonia or acetic acid was added to adjust pH value of TBT solutions measured by a pH meter; The solution (less than 2/3 volume) was heated and reacted in a hydrothermal autoclave (WDF-0.1L type, Weihai autocontrol reaction kettle Co. Ltd., China) after homogeneously mixed by magnetic stirrer, the autoclave's control voltage and mixing speed were fixed to 190 V and 250 rpm. The synthesized mono-dispersed precursor was put into a vacuum oven (vacuum degree, temperature was 0.03 MPa, 70 °C, respectively) after adding into traces of Triton x100 for 6 hrs, and then ground to TiO_2 nanoparticles.

Compared with traditional experimental design, orthogonal experiment design is beneficial for realizing prompt and accurate evaluation of optimal condition ratio with large quantity of factors and levels. Here, (*A*) temperature, (*B*) pH value, (*C*) reactive concentration and (*D*) reaction time were selected as the hydrothermal factors of orthogonal array $OA_9(3^4)$, for each factor, three levels were accordingly given. The experimental factors (*A*, *B*, *C*, *D*) and levels assigned for orthogonal experiments were listed in Table 2. 9 samples were synthesized according to $OA_9(3^4)$ orthogonal experimental table.

Table 2 Factors and levels selected for orthogonal experiment.

Level	*A*: TBT concentration(%)	*B*: pH value	*C*: reactive temperature(°C)	*D*:reactive time (hrs)
1	5	6.0	80	2
2	10	9.0	120	3
3	15	11.0	160	4

In general, clearer and sharper peaks of TiO_2 XRD pattern effectively reflect higher degree of crystalline; smaller particle diameters of TiO_2 nanoparticles mean larger surface areas, which both contribute to higher photocatalytic properties. Therefore, crystalline phase and particle size of TiO_2 nanoparticles are two main parameters to determine the optimal experimental ratio. The crystalline phase of TiO_2 nanoparticles were determined by XRD diffractometer (D8 advance type, Bruker AXS Co. Ltd., Germany), and their *S*/*V* values (m^2/cm^3) were measured through a laser scattering particle analyzer (Rise-2006 type, Beijing Liuyi Apparatus Co. Ltd., China), which can effectively represent equivalent diameter of TiO_2 nanoparticles based on Rayleigh scattering Formula 1.

$$I = \frac{24\pi^3 NV^2(n_1^2 - n_2^2)}{\lambda^4(n_1^2 + n_2^2)} I_0 \quad (1)$$

where, *N* is particles population per unit volume; *V* is the volume of single particle; *I*, I_0 stands for intensity of the scattered and incident light; n_1, n_2 represents refractive index of particle and disperse medium.

The microscale morphology of nanoscale TiO_2 powder, TiO_2/concrete composite sample was observed with SEM (S3500N type, Hatchi, Japan) after oven-dried, or/and top surface Au-sprayed, respectively.

Finally, an experimental confirmation was carried out using the predicted optimum levels obtaining from a comprehensive consideration on the results of TiO_2 nanoparticles under 4 factors with 3 levels, in order to verify that the optimum conditions suggested by the matrix experiments do give the enhancement.

2.3 Fabrication of TiO_2/concrete composite

Presently, synthetic methods of photocatalytic concrete include direct spraying[10], pre-coating aggregate[11] and photocatalytic cement mortar covering[12]. Here TiO_2/concrete composite was fabricated through directly spraying TiO_2 suspension on a porous concrete substrate.

The procedures of TiO_2 suspension preparation were as follows. Firstly, a trace of Triton x100 (0.5%) was dissolved in distilled water, and TiO_2 nanoparticles with varied concentrations (c_{TiO2}=0, 0.5, 1.0, 2.0, and 3.0 g/L) were added. Then the pristine TiO_2 suspension was firstly stirred by a magnetic stirrer (200 rpm, 40 min) and subsequently ultrasonic treated for 15 min (40 kHz, 60 W) by a sonicator (KQ2200B type, Jiangsu Kunshan Ultrasonic Instruments Co., Ltd., China).

The porous concrete was prepared by mixing large quantity of bubble generated from H_2O_2 foaming agent into thin cement slurry with water-cement-ratio of 0.8 and sodium aluminate of 1.3% to cement amount, similar to our previous works[8]. Then, 28 d-cured porous concrete cubic specimen was cut into porous concrete substrate with appropriate size with 70.7 mm×70.7 mm×20 mm, and put into a culture dish, and 10 mL TiO_2

suspension was sprayed evenly on its top surface by a sprayer. After sufficient absorbing and drying, TiO_2/concrete composite surface was rubbed with 360 mesh fine sandpapers, and rinsed under running distilled water, to remove weak adhesion of TiO_2 nanoparticles.

2.4 Photocatalytic characterization of TiO_2 nanoparticles and TiO_2/concrete composite

MeO is an azo dye of 4-[4-(dimethylamino) phenylazo] benzenesulfonic acid sodium salt, which is sensitive, but hard to oxidized degradation under UV-radiation. Therefore, MeO was chosen for representing azo-pollutants largely existed in urban areas. Photocatalytic oxidation of MeO solutions is used for evaluating degradation ability of TiO_2[13]. Uv-vis spectrophotometry (755B type, Shanghai Precision Scientific Instrument Co. Ltd., China) was used to obtain MeO's absorption curve with different concentrations. In order to guarantee accuracy of measuring result, the standard curve about relationship between MeO's concentration and its maximum absorbance was also depicted.

It is established that the doped Ag^+ can affect catalytic oxidation through reducing nanoscale TiO_2's energy gap, forming "electron capture well", and improving separation of electron from hole while deposited on the TiO_2 surface. That is to say, Ag^+ is capable of promoting catalytic ability of TiO_2[14]. Therefore, Ag^+ addition, c_{TiO2} and MeO concentration are designed as three main factors to affect photocatalytic degradation of MeO solutions of TiO_2 nanoparticles and TiO_2/concrete composites. When exploring the influence of one factor (Ag^+ or MeO concentration) on photocatalytic activity of TiO_2 nanoparticles, the other two factors were fixed at constant, and the optimal ratio was achieved after analyzing MeO degraded curve. Then c_{TiO2} was selected as the variable factor, TiO_2/concrete composites to be measured were fabricated by mixing the optimal amount of Ag^+ and MeO, and the degradation curve was plot according to calculated results, and the optimal ratio was also achieved.

Before UV radiation, in the sunless room, TiO_2 nanoparticles were added into MeO or/and $AgNO_3$ aqueous solution with different concentrations; Hereafter, each TiO_2 suspension was under magnetic stirred for 45 min, and sonication for 15 min, which was sufficient for MeO reaching equilibrated adsorption state on TiO_2 surface. TiO_2/concrete composite with five different c_{TiO2} was immersed in 2.5 mg/L MeO and 5% Ag^+ aqueous solution, respectively. The corresponding suspension with only TiO_2 nanoparticles or TiO_2/concrete composite was exposed to UV-radiation at λ=460 nm with an ultraviolet irradiation apparatus (WD-9403C type, Beijing Liuyi instrument factory, China), respectively.

During UV-radiation periods, 3 ml sample suspension was dipped out at a regular interval (30 min), and got rid of TiO_2 nanoparticles by centrifuging (5000 rpm, 15 min) through a low-speed desktop centrifuge (TDL-60B type, Shanghai Anting Scientific Instrument Factory, China). Removal of MeO was determined through measuring the absorbance value (λ=460 nm), using the UV-vis spectrophotometer. Absorbance value of sample before UV-radiation was read as A_0, and absorbance at regulated time was recorded as A_t. The formula used for calculating degradation rate of MeO solution was Formula 2.

$$\eta = \frac{A_t - A_0}{A_0} \times 100\% \quad (2)$$

where, A_0 is initial absorbance, and A_t is absorbance of MeO solution when $T=t$.

3. Results and discussions

3.1 The optimal ratio of synthesis parameters of TiO_2 nanoparticles

XRD patterns of TiO_2 nanoparticles in group No. *A*2, *A*5, *A*7 and *A*8 are typically showed in Fig. 1, and the main peak (*MP*) and particles size (*S*/*V*) of anatase phase TiO_2 are shown in Table 3. It's worth to pointing out that "0" means amorphous TiO_2 nanoparticles are synthesized. The calculated values of analysis of mean (*ANOM*) and the maximal range (*R*) by range analysis method are correspondingly given in the Table 4.

As revealed in Table 3 & Fig. 1, anatase TiO_2 is successfully synthesized only in 3 samples (*A*2, *A*5 and *A*7). Obvious characterized peaks of anatase TiO_2 (2θ=25.3°, 36.9°, 37.8°, 38.6°, 48.0°, 53.9° and 55.1°) are emerged, which represent (101), (103), (004), (112), (200), (105) and (211) patterns of TiO_2. These indicate that the phase of TiO_2 nanoparticle using optimal hydrothermal reactive condition can be only anatase without any rutile and brookite synthesized.

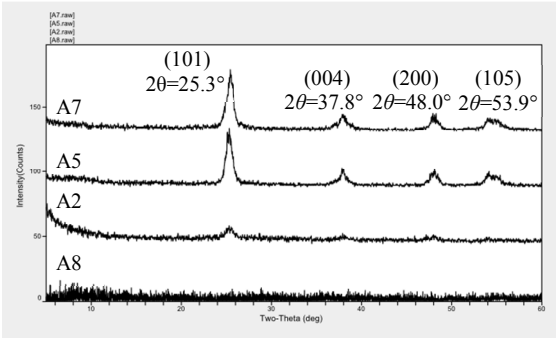

Fig.1 XRD patterns of synthesized TiO_2 nanoparticles in group No. *A*2, *A*5, *A*7, and *A*8

Table 3 Main peak (*MP*) and particles size (*S*/*V*) results of orthogonal experiment of synthesized TiO_2 nanoparticles.

Factors / No.	*A* (%)	*B*	*C* (°C)	*D* (hrs)	*MP* (2θ=25.3°)	*S*/*V* (m^2/cm^3)
A1	1(5)	1(6)	1(80)	1(2)	0	45.570
A2	1(5)	2(9)	2(120)	2(3)	18	63.717
A3	1(5)	3(11)	3(160)	3(4)	0	21.145
A4	2(10)	1(6)	2(120)	3(4)	0	10.526
A5	2(10)	2(9)	3(160)	1(2)	41	20.086
A6	2(10)	3(11)	1(80)	2(3)	0	16.901
A7	3(15)	1(6)	3(160)	2(3)	49	23.271
A8	3(15)	2(9)	1(80)	3(4)	0	57.143
A9	3(15)	3(11)	2(120)	1(2)	0	18.765

Taking the *MP* results of the orthogonal experiment shown in Table 3 for instance, the data processing of *ANOM* and *R* by range analysis method is shown as follows. For each factor in the mean value M_1 row, the test results consisting of level 2 are added and then divided by 3, which give the mean values of level 2, and so on. For example, the mean value for factor *C*

(*temperature*) at level 2 is (18 + 41 + 0)/3 = 19.67. For each factor, the corresponding maximum value subtracted the minimum value amongst M_1, M_2 and M_3 produces each factor's range value R. It is found that the R of C (*temperature*) is higher than any other factor, indicating that holding temperature (C) has the highest impact on the response (*MP*) of anatase TiO_2, while contribution of TBT concentration (A) is negligible. According to variance analysis outcome (as revealed in Table 4), the variation of the response (*MP*) with 3 levels for different factors is depicted in Fig. 2. The higher mean value is, the better response (*MP*) is, therefore, the optimal reactive combination for response (*MP*) are $A_3B_2C_3D_2$, as revealed in Table 4 and Fig. 2. In other words, the optimum parameters are the TBT concentration at 15%, pH value at 9.0, reactive temperature at 160°C, reactive time at 3 hrs.

Table 4 The *AVOM* and *R* according to *MP* and *S*/*V* results.

Range analysis	Factors of *MP* (2θ=25.3°)				Factors of *S*/*V* (m^2/cm^3)			
	A	*B*	*C*	*D*	*A*	*B*	*C*	*D*
M_1	6	16.33	0	13.67	43.477	26.456	39.871	28.140
M_2	13.67	19.67	6	22.33	15.838	46.982	31.003	34.630
M_3	16.33	0	30	0	33.060	18.937	21.501	29.604
R	10.33	19.67	30	22.33	27.640	28.045	18.371	6.489
Factor order	*C*(reactive temperature)>*D*(reaction time)>*B*(pH value)>*A*(TBT concentration)				*B*(pH value)>*A*(TBT concentration)>*C*(reactive temperature)>*D*(reaction time)			
Optimization level	A_3	B_2	C_3	D_2	A_1	B_2	C_1	D_2
Optimum combination	$A_3B_2C_3D_2$				$A_1B_2C_1D_2$			

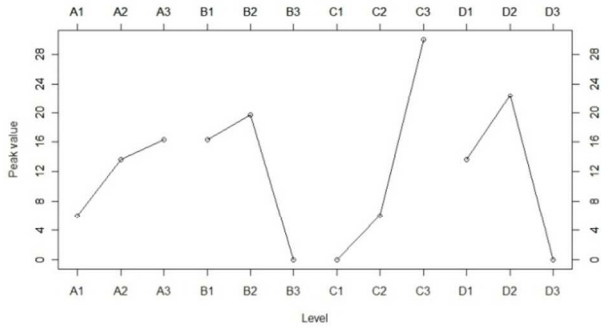

Fig. 2 Variation of the main peak of TiO_2 nanoparticles with different levels for each factor

In order to further investigate which factors significantly affect the *MP* and *S*/*V*, the analysis of variance (*ANOVA*) of *MP* and *S*/*V* values was studied and the calculated results are represented in Table 5. The number of levels (3) subtracted 1 gave the degree of freedom (*DOF*). The sum of squares was acquired by Formula 3.

$$SS_i = 3((M_{1i} - M)^2 + (M_{2i} - M)^2 + (M_{3i} - M)^2) \quad (3)$$
$$(i = A, B, C, D)$$

where, SS_i stands for the sum of squares, and M stands for the 9 mean values. Sum of squares divided by degree of freedom produced mean squares (M_i).

Table 5 *ANOVA* results according to *MP* and *S*/*V* shown in Table 4.

Factors	*DOF*	*MP*(2θ=25.3°) SS_i	M_i	F_i	$Pr(>F_i)$	Factors	*S*/*V* (m^2/cm^3) SS_i	M_i	F_i	$Pr(>F_i)$
A	2	172.61	86.31	1.00	-	*A*	116 9.03	584.51	16.815	0.056*
B	2	664.67	332.33	3.85	0.206	*B*	126 4.37	632.19	18.186	0.052*
C	2	151 2.00	756.00	8.76	0.102	*C*	506.39	253.19	7.284	0.121
D	2	760.67	380.33	4.41	0.185	*D*(residual)	69.52	34.76	1.00	-

Noting that, "*" represents significant factor.

Size optimization is also essential. Fig. 3 (range analysis) demonstrates that $A_1B_2C_1D_2$ is the best composition for the response (*S*/*V*). Variance analysis in Table 4 shows that influence degree ranking of four factors is: $B>A>C>D$. pH value (B), reaction time (D) has a top, bottom influence on *S*/*V* value, respectively.

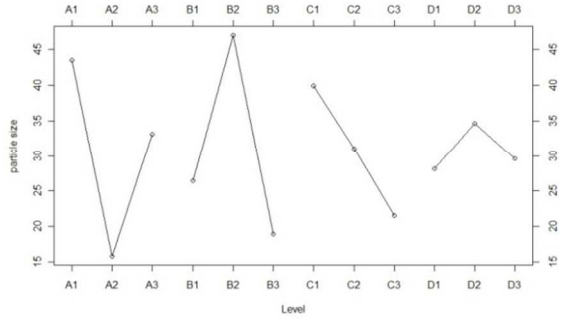

Fig. 3 Variation of the *S*/*V* of TiO_2 nanoparticles with different levels for each factor

TBT concentration (A) and reactive temperature (C) come to different conclusion about the optimal ratio. It is noted that two mean size values in group No. $A1$ and $A3$ have little distinction. TBT concentration (A) has a significant impact on TiO_2 nanoparticles synthesis according to *ANOVA* of particles size. Therefore, allowing for the cost, 5.0% TBT concentration (A_1) is the optimum. For reactive temperature's selection, it is impossible to achieve anatase TiO_2's synthesis at 80 °C. Therefore, 160°C (C_3) is the final holding temperature.

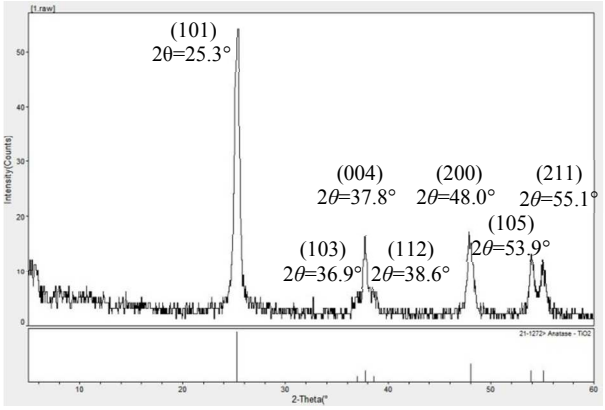

Fig. 4 XRD pattern of TiO_2 nanoparticles with optimal ratio

Consequently, $A_1B_2C_3D_2$ combination is selected as the optimal reaction condition. Fig. 4 shows XRD pattern of $A_1B_2C_3D_2$ verification sample, in which the diffraction peaks (2θ=25.3°, 36.9°, 37.8°, 38.6°, 48.0°, 53.9° and 55.1°) well match anatase TiO_2. Furthermore, most of TiO_2 nanoparticles present as mono-dispersed polygons with distinct crystalline phases, some even near spherical shapes, notwithstanding some soft but small aggregations, as revealed in Fig.5. A large number of TiO_2 nanoparticles are approximately 130 nm, which are consistent to *S*/*V* equivalent diameters of *A*7 group, acquired from the laser scattering particle analyzer, as shown in Table 3.

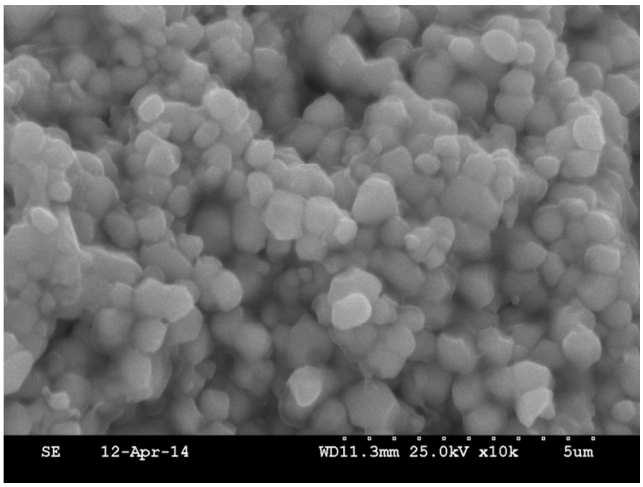

Fig. 5 SEM microstructure of TiO_2 nanoparticles with optimal ratio

3.2 Photocatalytic activity of TiO_2 nanoparticles

The absorbance value of pristine TiO_2 nanoparticles suspension after sonication for 15 min with 1.0% c_{TiO2} along with varied UV wavelength is depicted in Fig.6. The maximal, secondary high absorbance of pristine TiO_2 nanoparticles appears at λ=470 nm, 280 nm, respectively, as demonstrated in Fig.6.

As showed in Fig. 7, MeO has the strongest photoabsorption when λ=460 nm, where pristine TiO_2 nanoparticles also has maximalabsorbency . According to Longbow-Bill's law, the absorbency of the solutions has a linear relationship with their concentration. Linear fitting in Fig. 8 guarantees the accuracy of UV spectrophotometer. Linear fitting in Fig. 8 shows a high coincidence between measuring and fitting curve.

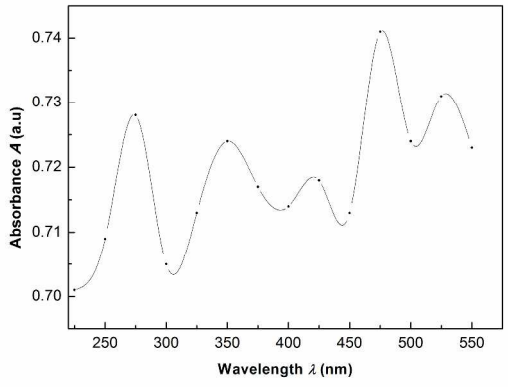

Fig. 6 UV-Vis spectra of pristine TiO_2 nanoparticles

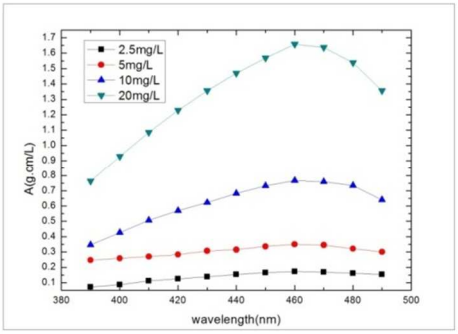

Fig. 7 Absorption curves of MeO solutions with various concentration

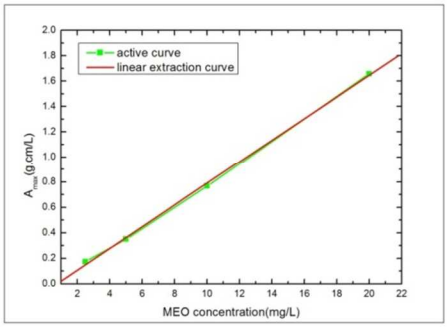

Fig. 8 Calibrating curve of MeO solutions

Ag^+ is proposed with a prominent enhancement for photo-oxidation activity of TiO_2 nanoparticles. It is assumed that Ag^+ may be beneficial to form "electron capture well" when deposited on TiO_2 surface, and to improve separation of electron from hole[15]. Degradation rate of MeO solutions was tested by adjusting MeO concentration and Ag^+ incorporation. Other reactive conditions were fixed (λ= 284 nm, pH=6 and c_{TiO2}=2.0 g/L). The detailed experimental reactant ratio was displayed in Table 6.

Table 6 Seven items on proportions of MeO concentration and Ag^+ addition for optimizing photocatalysis of TiO_2 nanoparticles.

Item No.	MeO concentration (mg/L)	Ag^+ addition (%)
M1	10	0
M2	10	1
M3	10	3
M4	10	5
M5	2.5	5
M6	5	5
M7	20	5

Fig. 9 shows the influence of Ag^+ additive amount for MeO photo-degradation. Compared with pure TiO_2 nanoparticles, Ag^+ addition displays a striking promotion to degradation rate of MeO solution (or improvement of degradation rate of MeO solution is induced by Ag^+ addition). MeO degradation level increases along with increase of Ag^+ addition. The majority of MeO was degraded in the first 3 hrs for all Ag^+ addition. 25% MeO was degraded when 5.0% Ag^+ was added in the mixture; however, only 4.0% MeO realizes its oxidative degradation without Ag^+ addition.

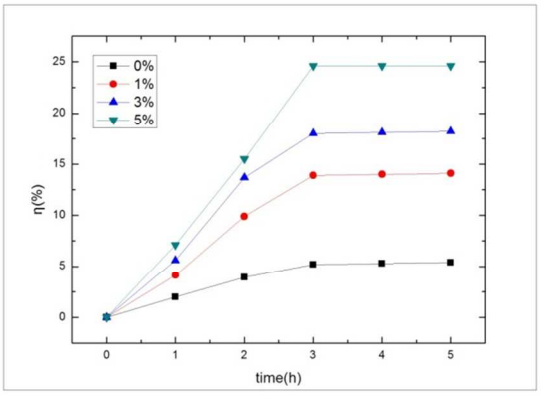

Fig. 9 Photocatalytic degradation curves of TiO_2 nanoparticles with variable Ag^+ additions

Fig.10 shows the influences of MeO concentration for photocatalytic activity of TiO_2 nanoparticles. Four samples were tested under the same conditions (λ=284 nm, pH=6.0 and c_{TiO2}=2.0 g/L). Most of the samples are degraded in the first 3 hrs and reach their maximum degradation rate. As the MeO concentration decreases, degradation degree of MeO increases. After 3 hrs irradiation, the degradation ratio with 2.5 mg/L MeO is nearly 60%. Higher MeO concentration bring forth lower MeO degradation ratio, as a result from that certain amount of nanoscale TiO_2 is capable of oxidizing fixed quantitative MeO at fixed light intensity. Therefore, excess MeO can not be thoroughly degraded with insufficient catalyst.

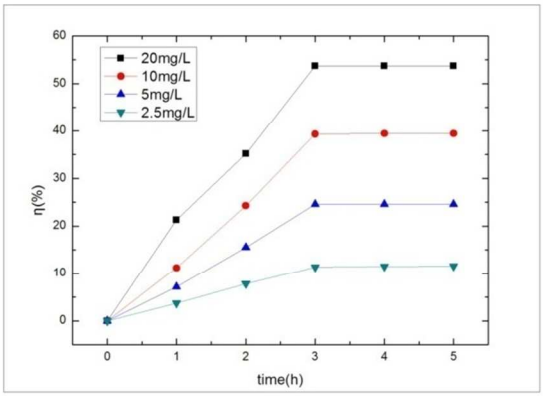

Fig. 10 Photocatalytic degradation curves of TiO_2 nanoparticles with variable MeO concentrations

3.3 Photocatalytic activity of TiO_2/concrete composite (photocatalytic concrete)

As above mentioned, 2.5 mg/L MeO solution realizes its highest degradation ratio with 5.0% Ag^+ addition, 284 nm UV-radiation and acidic environment (pH=6.0), and the corresponding TiO_2 nanoparticles has the best catalytic activity. Therefore, influence of varied c_{TiO2} for MeO degradation ratio by TiO_2/concrete composite was explored with fixed aforementioned conditions. The final fabricated TiO_2/concrete composite with 1.0 g/L c_{TiO2} is immersed in 2.5 mg/L MeO mixed solution on the culture dish (Fig. 11), the corresponding microscale morphology is depicted in Fig.12.

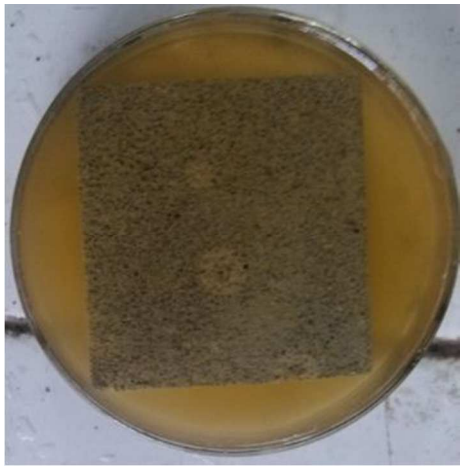

Fig. 11 Photograph of fabricated TiO_2/concrete composite immersed in MeO solution

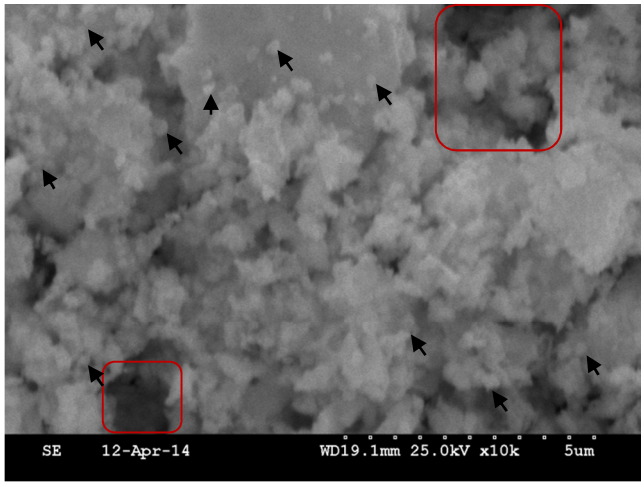

Fig. 12 SEM image inside a macropore peephole of TiO_2/concrete composite with 1.0 g/L c_{TiO2} (black arrows--deposited TiO_2 nanoparticles; red rectanglulars—microscale pores)

As revealed in Fig.s 11 & 12, porous concete substrate possesses mult-scale pore structures with both large quantity of macropores necessary for TiO_2 suspension infiltration, and considerable macropores essential for TiO_2 nanoparticles adsorption & deposition. TiO_2 nanoparticles are mono-dispersed and dotted among relatively loose cement hydration, mainly C-S-H gels.

Photocatalytic activity of TiO_2/concrete composite is explored through analyzing transformation of MeO degradation ratio. MeO degraded curves of TiO_2/concrete composite with different c_{TiO2} are showed in Fig. 13. According to degradation curve, up to 35% MeO can be oxidized when there are 5% Ag^+, 2.5 mg/L MeO and 2.0 g/L TiO_2 in the mixture. However, the enhancement effect of c_{TiO2} is less remarkable, since TiO_2/concrete composite with 0.5 g/L c_{TiO2} possibly achieves almost 24% MeO degraded ratio.

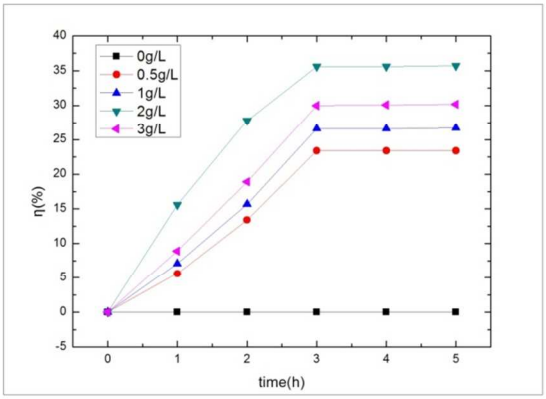

Fig. 13 Photocatalytic degradation curves of TiO_2/concrete composite with variable c_{TiO2}

It is worth to pointing out that TiO_2 nanoparticles have the best photocatalytic property under UV radiation. However, it is assumed that TiO_2/concrete composite is applied under sunlight, so it is necessary to further widen absorption wavelength range. Doping N ion, P ion, ZnO, or ZnS sources with different absorption range can be practicable[3], and can be also helpful to improve MeO degradation rate. Therefore, high photocatalytic active concrete with wide absorption range is required, and our group will conduct the related experiment in the near future.

Conclusions

(1) Through orthogonal range & variance analysis of XRD main peaks and scattering *S*/*V* values, the optimal anatase TiO_2 nanoparticles are hydrothermal synthesized in TBT concentration of 5%, pH value of 9.0, reactive temperature of 160°C, and reactive time of 3 hrs.

(2) Photocatalytic properties of TiO_2 nanoparticles, sprayed TiO_2/concrete composite reach the maximal value (54%, 35.7%) with the optimal ratio of Ag^+ addition in 5%, pH in 6.0, MeO concentration in 2.5 mg/L, and c_{TiO2} in 2.0 g/L, respectively.

(3) Microstructures reveals sprayed TiO_2/concrete composite has mult-scale pore structures, which are simutaneously apt to TiO_2 suspension infiltration and strong adsorption & deposition onto cement hydration of TiO_2 nanoparticles.

Acknowledgements

This work was supported by grants from NSFC (No. 51208272, 51378270) & NSFC of International Cooperation Fund (Item No. 51420105015) and Shangdong Province Young and Middle-Aged Scientists Research Awards Fund (Item No. BS2013CL017).

Notes and references

[a]*P.O. Box 221, Fushun Rd.11, Shibei District, Qingdao, P.R.China. Fax: 86 532 8507 1276; Tel: 86 532 8507 1275; E-mail: lawjanelim2009hit@gmail.com*
[b]*Xueyuan Rd.37, Haidian District, Beijing, P.R.China. Fax: 86 10 8231 7132; Tel: 86 10 8231 7132; E-mail: 503805014@qq.com*

1 (a) A. Hagfeldt and M. Gratzel, *Chem. Rev.* 1995, **95**(1), 49; (b) R. Asahi, T. Morikawa, T. Ohwaki, K. Aoki and Y. Taga, *Science* 2001, **293**(5528), 269; (c) A. L. Linsebigler, G. Q. Lu and J. T. Yates, *Chem. Rev.* 1995, **95**(3), 735; (d) M. R. Hoffmann, S. T. Martin, W.Y. Choi and D.W. Bahnemann, *Chem. Rev.* 1995, **95**(1), 69; (e) C.H. Chen, Q.W. Liu, S.M. Gao, K. Li, H. Xu, Z.Z. Lou, B.B. Huang and Y. Dai, *RSC Adv*. 2014, **4**: 12098.

2 (a) A. Folli, C. Pade, T.B. Hansen, T. De Marco and D.E. Macphee, *Cem. Concr. Res.* 2012, **42**(3), 539; (b) M.M. Hassan, H. Dylla, L.N. Mohammad and T. Rupnow, *Construc. Build. Mater.* 2010, **24**, 1456; (c) S. S. Lucas, V. M. Ferreira, and J. L. Barroso de Aguilar, *Cem. Concr. Res.* 2013, **43**, 112; (d) M. Horgnies, I. Dubois-Brugger and E.M. Gartner, *Cem. Concr. Res.* 2012, **42**, 1348; (e) A. Maury-Ramirez, W. De Muynck, R. Stevens, K. Demeestere and N. De Belie, *Cem. Concr. Compos.* 2013, **36**, 93.

3 (a) G. Husken, M. Hunger and H. J. H. Brouwers, *Build. Environ.* 2009, **44**(12), 2463; (b) R. Sugranez, J.I. Alvarez, M. Cruz-Yusta, I. Marmol, J. Morales, J. Vila and L. Sanchez, *Build. Environ.* 2013, **69**, 55; (c) S.Y. Guo; S. Han, H.F. Mao, C.C. Wu, L.C. Jia, B. Chi, J. Pu and L. Jian, *J. Alloys Compd. 2012*, **544**(15): 50; (d) M.M. Ballari, Q.L. Yu, and H.J.H. Brouwers, *Catal. Today* 2011, **161**, 175.

4 (a) A. Maury-Ramirez, K. Demeestere and N. De Belie, *J. Hazard. Mater.* 2012, **212**, 218; (b) J. M. Herrmann, *Catal. Today* 1999, **53**(1), 115; (c) A. Fujishima, X. Zhang and D. A. Tryk, *Surf. Sci. Rep.* 2008, **63**(12), 515; (d) A. K. Kole, C. S. Tiwary and P. Kumbhakar, *Cryst. Eng. Comm.* 2013, **15**, 5515.

5 (a) M. Hussain, R.Ceccarelli, D. L.Marchisio, D. Fino, N. Russo and F. Geobaldo, *Chem. Eng. J.* 2010, **157**(1):45; (b) B. Souvereyns, K. Elen, C. De Dobbelaere, A. Kelchtermans, N. Peys, J. Dhaen, M. Mertens, S.Mullens, H. Van den Rul, V. Meynen, P. Cool, A. Hardy and M. K. Van Bael, *Chem. Eng. J.* 2013, **223**:135; (c) N. Uekawa, J. Kajiwara, K. Kakegawa and Y. Sasaki, *J. Colloid Interf. Sci* . 2002, **250**(2), 285.

6 (a) D. V. Bavykin, J. M. Friedrich and F. C. Walsh, *Adv Mater* 2006, **18**(21), 2807; (b) D. V. Bavykin, V. N. Parmon, A. A. Lapkin and F.C. Walsh, *J. Mater. Chem.* 2004, **14**(22), 3370; (c) H. Cheng, J. Ma, Z. Zhao and L. Qi, *Chem. Mater.* 1995, **7**(4):663; (d) K. Hashimoto, H. Irie and A. Fujishima, *AAPPS Bulletin* 2007, **17**(6):12.

7 (a) J. Chen and C. S. Poon, *J. Environ. Manage.* 2009, **90**(11), 3436; (b) L. Senff, D. M. Tobaldi, S. Lucas, D. Hotza, V. M. Ferreira and J. A. Labrincha, *Compos. Part B-Eng.* 2013, **44**(1), 40; (c) M. Smits, C. K. Chan, T. Tytgat, B. Craeye, N. Costarramone, S. Lacombe and S. Lenaerts, *Chem. Eng. J.* 2013, **222**, 411.

8 (a) A.M. Ramirez, K. Demeestere, N. De Belie, T. Mantyla and E. Levanen, *Build. Environ.* 2010, **45**(4), 832; (b) S.H.Shen, M. Burton, B. Jobson and L. Haselbach, *Constr. Build. Mater.* 2012, **35**, 874; (c) J.L.Luo, Q.Y. Li, T.J. Zhao, S. Gao, S.W. Sun and L. Chen, *Nanosci. Nanotechno. Lett.* 2014, **6**(1), 72.

9 (a) M. Jalal, M.Fathi and M. Farzad, *Mech. Mater.* 2013, **61**, 11; (b) A. Nazari, *Mater. Struct.* 2010, **44**(4), 773; (c) A. Nazari and S. Riahi, *Mater. Sci. Eng. A-Struct.* 2010, **528**(2), 756.

10 R. Thiruvenkatachari, T. O. Kwon and I. S. Moon, *Korean J. Chem. Eng.* 2005, **22**(6), 938.

11 (a) M. Chen and J.W. Chen, *J. Clean. Prod.* 2011, **19**, 1266; (b) C. S. Poon and E. Cheung, *Constr. Build. Mater.* 2007, **21**(8), 1746.

12 (a) M. M. Hassan, H. Dylla, S. Asadi, L. N. Mohammad and S. Cooper, *J. Mater. Civil. Eng.* 2012, **24**(5), 599; (b) D. Osborn, M. M. Hassan and H. Dylla, *Transport. Res. Rec.* 2012, **2290**, 147.

13 (a) Y. S. Sohn, Y. R. Smith, M. Misra and V. Subramanian, *Appl. Catal. B-Environ.* 2008, **84**, 372; (b) N. Guettai and H. Ait Amar, *Desalination* 2005, **185**, 439.

14 (a) A. Sclafani, L. Palmisano and E. Davi, *J. Photoch. Photobio. A* 1991, **56**(1), 113; (b) M. M. Kondo and W. F. Jardim, *Water Res.* 1991, **25**(7), 823; (c) Y. X. Tang, P. X. Wee, Y. K. Lai, X. P. Wang, D. G. Gong, P. D. Kanhere, T. T. Lim, Z. L. Dong and Z. Chen, *J. Phys. Chem. C* 2012, **116**(4), 2772.

15 (a) Z. X. Ji, M. N. Ismail, D. M. Callahan, E. Pandowo, Z. H. Cai, T. L. Goodrich, K. S. Ziemer, J. Warzywoda and A. Sacco, *Appl. Catal. B-Environ.* 2011, **102**(1-2), 323; (b) J. Okumu, C. Dahmen, A. N. Sprafke, M. Luysberg, G. von Plessen and M. Wuttig, *J. Appl. Phys.* 2005, **97**(9), 094305.